Thermalization of fast cesium $5D_{3/2}$ atoms in collisions with ground-state cesium atoms

A. Marks,[1] A. P. Hickman,[1] A. D. Streater,[2] and J. Huennekens[1]
[1]*Department of Physics, Lehigh University, Bethlehem, Pennsylvania 18015, USA*
[2]*Research Electro-Optics, 5505 Airport Boulevard, Boulder, Colorado 80301, USA*
(Received 18 May 2004; published 19 January 2005)

We have investigated collisions involving fast, excited Cs atoms produced by photodissociating Cs_2 molecules with a pulsed dye laser. The velocities of the atoms in the $5D$ state formed by the process $Cs_2(X\,^1\Sigma_g^+)+\hbar\omega_{\text{pump}}\rightarrow Cs_2^*\rightarrow Cs(5D)+Cs(6S)$ are much greater than typical thermal velocities associated with the cell temperature. Using a narrow-band cw probe laser to observe the increased Doppler broadening of the $5D_{3/2}\rightarrow 5F_{5/2}$ excitation line shape, we are able to monitor the time evolution of the velocity distribution of these $5D$ atoms. We analyze the data using a model that predicts the time-dependent excitation line shape of the fast atoms. Because the photons used to dissociate the molecules have a well-defined energy, the velocity distribution of the excited atoms in the early time after they are produced can be fairly well determined. Over time, velocity-changing collisions with ground-state Cs atoms cause the velocity distribution of excited atoms to approach the thermal limit. An analysis based on the strong-collision model leads to a prediction that the observed line shape at intermediate times will be a linear combination of contributions from distinct "fast" and "thermalized" atomic populations. By fitting our data to this model, a rate coefficient for velocity-changing collisions of fast $Cs(5D_{3/2})$ atoms with ground-state Cs atoms has been determined. The result $k_{\text{VCC}}=(6.1\pm1.2)\times10^{-10}$ cm^3 s^{-1} corresponds to an effective velocity-changing collision cross section of $\sigma_{\text{VCC}}^{\text{Cs,eff}}=(1.2\pm0.2)\times10^{-14}$ cm^2.

DOI: 10.1103/PhysRevA.71.012711 PACS number(s): 33.80.Gj, 32.70.Jz

I. INTRODUCTION

Photodissociation of molecules into fast, excited atoms using a tunable laser provides a technique for producing atoms with well-defined velocities for collision studies. The present work represents our first attempt to develop this concept into a useful technique. We demonstrate that fast, excited Cs atoms with a known velocity distribution can be produced through photodissociation of Cs_2 molecules, and we then observe the evolution of the excited atom velocity distribution due to velocity-changing collisions with ground state Cs atoms.

Photodissociation of Cs_2 molecules into ground- and excited-state cesium atoms has been observed since the early 1980s. Pioneering work was described in a series of papers by Collins and co-workers [1–6]. The process they studied may be written

$$Cs_2(X\,^1\Sigma_g^+)+\hbar\omega_{\text{pump}}\rightarrow Cs_2^*\rightarrow Cs(n\ell)+Cs(6S), \quad (1)$$

where $X\,^1\Sigma_g^+$ is the ground state of the cesium molecule and Cs_2^* represents an excited state or states that can be reached by a photon of energy $\hbar\omega_{\text{pump}}$. The identities of these excited molecular states are different for different dissociation products $Cs(n\ell)$ and will change with ω_{pump}. In general, they are not known, although possible assignments can be made using theoretical potentials. However, the dissociating molecular state must be either a state that is repulsive at all internuclear separations or a bound state that is pumped above its dissociation limit. In either case, the molecule splits apart into one excited- and one ground-state atom. The excess energy of the photon above the dissociation threshold goes into the kinetic energy of the resultant atoms. Collins *et al.* [2] speculated that photodissociation of Cs_2 molecules with blue light was caused by excitation to the $E\,^1\Pi_u$ molecular state ($7P+6S$ atomic limit), which then underwent predissociation to a repulsive $^3\Sigma_u^+$ state coupled to the $5D+6S$ dissociation limit. In addition, the group at Kobe University has done extensive work on the $C\,^1\Pi_u$, $D\,^1\Sigma_u^+$, and $2\,^3\Pi_u$ states that predissociate via the $2\,^3\Sigma_u^+$ state to the $6P+6S$ limit [7–12].

The excited atoms produced in the photodissociation process can be observed directly through the fluorescence they emit, by probe laser absorption, by probe-laser-induced ionization as in the work of Collins and co-workers [1–6], or by probe-laser-induced fluorescence (LIF). In the case of absorption, if the probe laser has a sufficiently narrow bandwidth (as in the present work), the velocity distribution of the fast, excited atoms can be inferred through the increase of the Doppler broadening of the absorption line shape. The technique of probing the velocity of excited-state atoms by observing the Doppler shift or Doppler broadening of associated spectral lines is called Doppler velocity spectroscopy and has been used for a wide range of atomic and molecular studies [13–18].

The excited atoms produced by photodissociation undergo thermalizing collisions with ground state Cs atoms and with other species. The study of velocity-changing collisions in general has proven to be a rich field [19–35]. Studies of velocity-changing collisions are essential in the understanding of such phenomena as the diffusion of atoms in a vapor [33], collision-broadened line shapes [21,27,28], and light-induced drift [23,24,26]. Since the details of velocity-changing collisions depend on the interaction between the colliding atoms, measurements of thermalization can yield important information about the interatomic potentials [30]. For ground-state atoms, velocity-changing collisions can be investigated through studies of atomic diffusion. For atoms

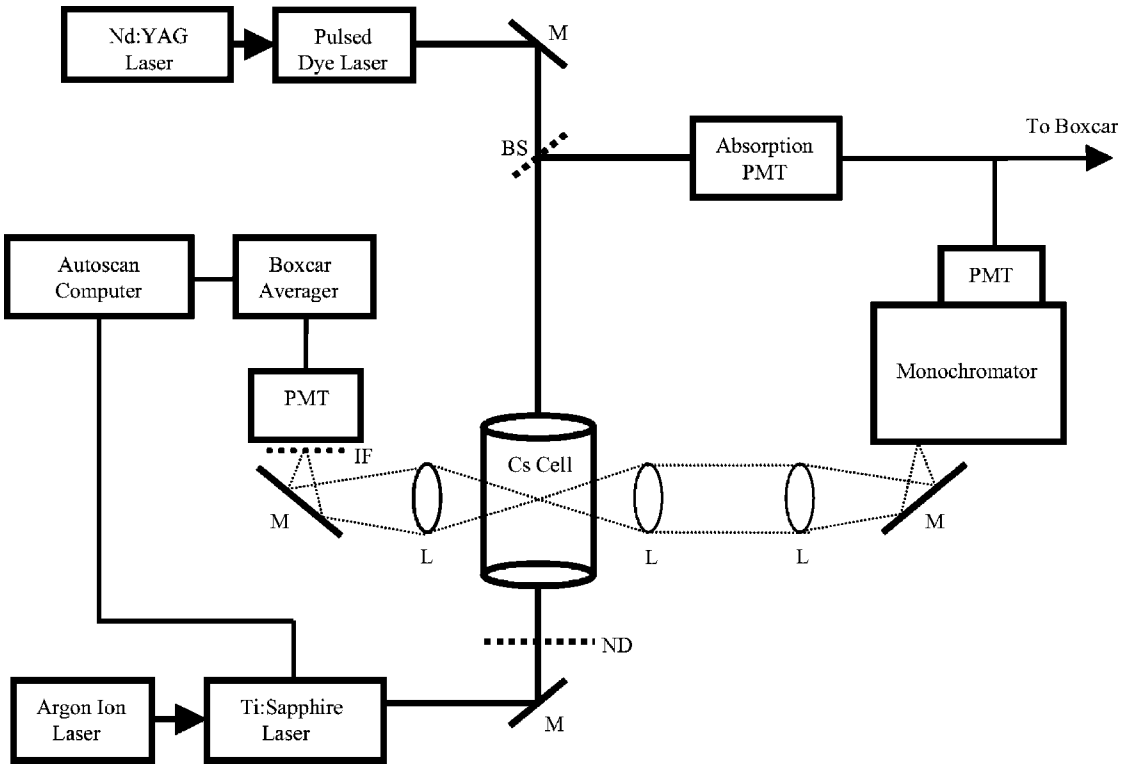

FIG. 1. Experimental setup. M, BS, L, ND, and IF represents mirror, beam splitter, lens, neutral density filter, and interference filter, respectively.

in excited states, short lifetimes generally preclude studies of this type. Therefore, velocity-changing collisions involving excited states have been studied primarily in two-step line shape [21,27] and light-induced drift [26] experiments.

In two-step line shape studies, a narrow-band laser is used to excite a single velocity group from within a thermal population. The thermalization of this selected velocity group is then monitored through the broadening of probe laser transitions to a more highly excited state as a function of density of the collision partner. While these studies have yielded much important information about velocity-changing collisions and their effects on line shapes, the range of velocities that can be selected is limited by the requirement that the laser detuning be within one or two Doppler widths of line center. This is because the wings of the spectral line are dominated by the Lorentzian function resulting from natural and pressure broadening. These wings have contributions at all frequencies from each velocity group and therefore provide no selectivity. For sodium at $T=500$ K, this requirement limits the range of velocities that can be studied to $v \leq 2\times10^5$ cm/s.

The technique we have developed goes beyond the usual pump-probe methodology, which typically yields either time-averaged line shape information (when two cw lasers are used) or time-resolved populations without line shape information (when two pulsed lasers are used). By using a pulsed laser to create fast atoms with a well-defined velocity distribution and then using a cw laser to probe the time-dependent thermalization, we obtain both the time resolution of the pulsed laser and the frequency resolution of the cw laser, so that time-resolved line shapes can be recorded [36].

This paper presents our results on the production of fast Cs($5D$) atoms by pulsed laser photodissociation of Cs_2 and the subsequent thermalization of the fast, excited atom population. By observing Doppler broadening of the Cs($5D_{3/2}$) $\rightarrow$Cs($5F_{5/2}$) excitation line shape using a narrow-band cw Ti:sapphire laser in a time-resolved fashion, we are able to monitor the velocity distribution of the excited Cs atoms as a function of time. Because high initial speeds can be accessed, this technique complements the two-step line shape studies. Our analysis provides a model for the line shape of the nascent fast atoms, including the homogeneous line shape due to natural broadening and optical pumping of the hyperfine levels, and Doppler broadening. We also formulate the expected time evolution of this line shape, using the strong-collision model [37]. The line shape is a time-dependent linear combination of contributions from "fast" and "thermalized" excited atoms. By fitting our data to this model, we determine effective rate coefficients and cross sections for velocity-changing collisions with an initial velocity of $\sim5\times10^4$ cm/s. For comparison, the mean thermal velocities are $\overline{v}=(2.6-2.8)\times10^4$ cm/s for our temperature range $T=161-226$ °C.

II. EXPERIMENT

A. Experimental setup

The current experimental setup is shown in Fig. 1. Cesium metal, contained in a sealed cylindrical Pyrex cell (Opthos Instruments) with a diameter of 25 mm and a length of 8 cm, was heated to temperatures in the range of

161–226 °C. At these temperatures the cesium atomic density ranges from 3.7×10^{14} to 4.5×10^{15} cm^{-3}, while the molecular Cs_2 density is in the range 3.4×10^{11} -1.2×10^{13} cm^{-3} [38]. A homemade, tunable, pulsed dye laser, pumped by the third harmonic (355 nm) of a Spectra-Physics DCR-11 Nd:YAG laser, was used to photodissociate Cs_2 molecules. Using Coumarin 480 dye, the laser typically produces 6 ns pulses at 10 Hz, with energies between 20 and 50 μJ, in the wavelength range from 463 to 497 nm. The multimode laser linewidth was determined to be ~30 GHz using a series of solid etalons. The pulsed dye laser was used to pump Cs_2 molecules to a repulsive state (or to the repulsive wall of a bound state above its dissociation limit) that dissociates to the $6S_{1/2}+5D_J$ atomic dissociation limits or to a bound state that predissociates to these limits [2,3]. A Coherent Model 899-29 cw Ti:sapphire laser, pumped by 10 W from an argon ion laser, produces 100–900 mW of power near 800 nm, with a linewidth of <1 MHz. This laser was used as a probe to further excite the $5D$ atoms to the $5F$ state. Typically, we chose $5D_{3/2}\rightarrow5F_{5/2}$ as the probe transition. Neither laser beam was focused in this experiment.

Fluorescence was detected at right angles to the Cs cell by one of two detectors. The first detector is a Hamamatsu R928 photomultiplier tube (PMT) attached to the output of a Spex 1681, 0.22-m monochromator. The monochromator resolution is 3.6 nm/mm, with a 1200 lines/mm grating blazed at 500 nm, and slit widths of 50 μm to 2 mm were used to obtain reasonable signal to noise with acceptable resolution. Resolved fluorescence was recorded by scanning the monochromator with both lasers held at fixed frequencies. Alternatively the monochromator was set to transmit $5F_{5/2,\ 7/2}\rightarrow5D_{5/2}$ atomic fluorescence while the probe laser was scanned over the $5D_{3/2}\rightarrow5F_{5/2}$ transition to obtain excitation spectra. In this latter application, the monochromator acts as a filter to isolate fluorescence from the $5F$ state. The second detector is a free standing PMT (Hamamatsu R928) with an interference filter [$\lambda_0=811$ nm, 8.7 nm full width at half maximum (FWHM) bandpass] attached to the front of the detector mount. With this detector, total broadband fluorescence on the $5F_{5/2,7/2}\rightarrow5D_{5/2}$ transitions (808.2 nm) was recorded while scanning the Ti:sapphire (probe) laser over the $5D_{3/2}\rightarrow5F_{5/2}$ transition (801.8 nm). Combinations of Schott NG-5, NG-4, and NG-3 neutral density filters were placed in the Ti:sapphire beam before the Cs cell to reduce the power to 100–150 mW (beam radius ~1 mm) in order to reduce power broadening of the spectral lines without too much loss of signal to noise.

A third PMT (Hamamatsu R2368) was used to detect the Ti:sapphire laser intensity transmitted through the cell. These transmission (or absorption) measurements were used to determine the density of $5D$ atoms that was produced through molecular photodissociation. In this case, NG-1, NG-10, and NG-3 neutral density filters were placed in the beam path before the cell to protect the PMT and to ensure that the absorption remained in the weak field (linear) regime. For these measurements the probe laser power incident on the cell was in the tens of μW range. An RG 780 long pass filter and an 811-nm interference filter were placed in front of the detector to discriminate against scattered photodissociation laser light.

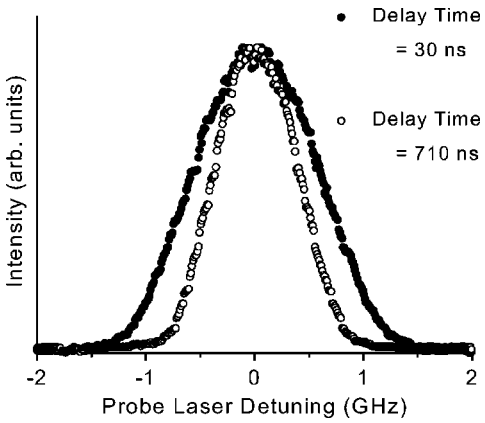

FIG. 2. $5F_{5/2,7/2}\rightarrow5D_{5/2}$ fluorescence signal recorded as the probe laser is scanned over the $5D_{3/2}\rightarrow5F_{5/2}$ transition. The fluorescence signals shown are for delays of 30 ns (●) and 710 ns (○) after the photodissociation pulse.

A Stanford Research Systems model 250 boxcar averager and gated integrator was used to process both fluorescence and absorption signals. The advantage of the boxcar is that it allows the averaging of signals associated with multiple dye laser pulses for each data point recorded, as well as the ability to set a gate to perform measurements within a certain time window. Electronic noise related to the firing of the pulsed Nd:YAG laser prevented clean signal acquisition during the first 20 ns after the pulsed laser fired. Thus the earliest fluorescence collection window we used began at a delay of 20 ns after the end of the dye laser pulse. The end of the photodissociation dye laser pulse was taken to be $t=0$. Timed excitation spectra were taken by scanning the cw probe laser over the $5D_{3/2}\rightarrow5F_{5/2}$ transition while the boxcar gate was set to monitor $5F_{5/2,7/2}\rightarrow5D_{5/2}$ fluorescence over a 20 ns interval. The time between the end of the dye laser pulse and the center of the boxcar detection window (which we will henceforth refer to as the "delay time") was varied for each scan in order to get a clear picture of the time evolution of the spectral line shapes. We observed that the decay of the fluorescence signal in time was consistent with the radiative lifetime of the cesium $5D$ state (1 μs), leading to the conclusion that no significant ionization was occurring due to the combined effects of both lasers. In addition, we used the monochromator to search for fluorescence from high-lying excited states other than $5D$ or $5F$ that would likely be produced by recombination of ions in the vapor. No such fluorescence was observed, thereby confirming that no significant ionization was taking place.

B. Experimental results

An example of our observations of the thermalization of fast, $Cs(5D_{3/2})$ atoms is shown in Fig. 2. The recorded signals represent $5F_{5/2,7/2}\rightarrow5D_{5/2}$ fluorescence as the probe laser was scanned over the $5D_{3/2}\rightarrow5F_{5/2}$ transition (excitation spectra) following pulsed laser photodissociation of Cs_2 molecules. Each data point represents an average over 30 shots of the pulsed dye laser. The $5D_{3/2}\rightarrow5F_{5/2}$ excitation line shape, recorded in the early time (~30 ns after the firing of

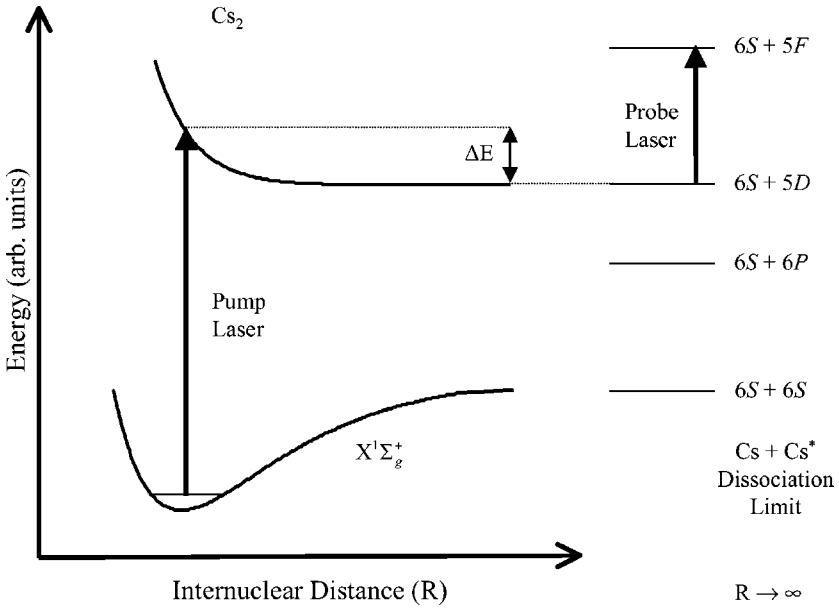

FIG. 3. Schematic diagram showing the production of fast, cesium 5*D* atoms using molecular photodissociation. The identity and shape of the upper dissociating state are not known (but see Sec. V).

the pulsed dye laser) before thermalizing collisions have had a chance to occur, is clearly broader (FWHM ~ 1.5 GHz) than the late time scan (~710 ns after the pulsed laser fires, FWHM ~ 1.0 GHz). This early time broadening is due to the fact that excited atoms produced through photodissociation have high speeds that lead to an increased Doppler broadening of the probe laser transition. As time goes on, the linewidth decreases due to thermalizing collisions that tend to reduce the speed of the excited atoms. Since the time necessary to thermalize the excited-atom speed distribution decreases with increasing cesium density (see Sec. IV), it is clear that collisions with other cesium atoms are at least partly responsible for the thermalization.

Data were taken at several different cell temperatures. The ground-state cesium density corresponding to each temperature was obtained from the vapor pressure curve of Nesmeyanov [38]. The probe laser was scanned over the $5D_{3/2} \rightarrow 5F_{5/2}$ transition and $5F_{5/2,7/2} \rightarrow 5D_{5/2}$ fluorescence was detected in a 20-ns window at a number of different delay times. For lower densities, the thermalization process takes longer, and delays up to 1 μs were used. At higher densities, delays up to only a few hundred nanoseconds were necessary. Three scans of the probe laser across the $5D_{3/2} \rightarrow 5F_{5/2}$ transition (~30 minutes each) were recorded for each delay time at each density in order to more accurately determine the linewidth.

III. THEORETICAL ANALYSIS

This section describes our analysis of the velocity distribution of fast atoms created by molecular photodissociation. This velocity distribution plays a crucial role in the interpretation of the probe laser excitation line shapes observed experimentally. We will discuss the effects of molecular motion and the thermal distribution of population over rovibrational levels of the molecule prior to photodissociation, natural (lifetime) broadening, pressure broadening, and optical pumping. The effects of thermalizing collisions after photodissociation are also included, using the strong collision model. We begin with a very simple model, and then we introduce the refinements necessary for a quantitative description of the experiments.

A. Simple model for the "top hat" line shape

We consider first the velocity distribution $f^{(0)}$ that would arise in the idealized, limiting case that all absorbing Cs_2 molecules are in the rovibrational ground state. We also assume that the molecules are at rest in the laboratory—that is, they have no center-of-mass translational motion—and that they dissociate isotropically. Finally, we neglect homogeneous broadening in this simple model.

Figure 3 illustrates the process we consider. A Cs_2 molecule is excited from a single rovibrational level of the electronic ground state to the continuum of levels associated with a hypothetical repulsive state that dissociates to the Cs(5*D*) + Cs(6*S*) separated atom limit. Photons with a broad range of energies can be absorbed, with probabilities determined by bound-free Franck-Condon factors [39]. If we let $\hbar\omega_{\text{pump}}$ be the energy of the pump laser photon and $E_{v,J}$ be the energy of the molecular rovibrational level of the electronic ground state before photodissociation, then the energy difference

$$\Delta E = \hbar\omega_{\text{pump}} + E_{v,J} - E_{5D+6S} \tag{2}$$

goes into translational energy of the resultant free atoms. Here the asymptotic energy of the dissociation limit (E_{5D+6S}) and all other energies will be referenced to the $v=0$, $J=0$ level of the Cs_2 molecular ground state. Since these atoms have equal masses (m), they share ΔE equally, and the speed v_{ph} each atom gains from the photodissociation process is given by

$$\frac{1}{2}\Delta E = \frac{1}{2}mv_{\text{ph}}^2. \tag{3}$$

In our ideal case, the dissociated atoms will all have the same speed, $v_{\text{ph}}=v_0$, where v_0 is determined from Eqs. (2) and (3) by setting $E_{v,J}=E_{0,0}=0$:

$$\Delta E = \hbar\omega_{\text{pump}} - E_{5D+6S} = mv_0^2. \tag{4}$$

Under these conditions, the distribution of velocities $\mathbf{v}_{\text{ph}}$ is

$$f^{(0)}(\mathbf{v}_{\text{ph}}) = \frac{1}{4\pi v_0^2}\delta(v_{\text{ph}} - v_0), \tag{5}$$

where $f^{(0)}(\mathbf{v}_{\text{ph}})d^3\mathbf{v}_{\text{ph}}$ is the probability that the excited $5D$ atom has acquired a velocity between $\mathbf{v}_{\text{ph}}$ and $\mathbf{v}_{\text{ph}}+d^3\mathbf{v}_{\text{ph}}$ as a result of the photodissociation process.

We now consider the $5D \rightarrow 5F$ probe laser absorption line shape that would result from this simple velocity distribution. When all homogeneous broadening effects (which will be considered in Sec. III D) are neglected, the absorption line shape $k_{5D\rightarrow 5F}(\Delta\omega)$ depends only on the Doppler broadening, which in turn depends on the distribution of the component of $5D$ atom velocities along the probe laser propagation direction defined by the probe laser wave vector $\mathbf{k}_{\text{L}}$. We can write

$$k_{5D\rightarrow 5F}(\Delta\omega) = N\int f^{(0)}(\mathbf{v}_{\text{ph}})\delta(\Delta\omega - \mathbf{k}_{\text{L}}\cdot\mathbf{v}_{\text{ph}})d^3\mathbf{v}_{\text{ph}}, \tag{6}$$

where $\Delta\omega \equiv \omega - \omega_0$ is the detuning of the probe laser frequency ω from the line center frequency ω_0 of the $5D \rightarrow 5F$ transition, $|\mathbf{k}_{\text{L}}| = \omega_0/c$, and N is a normalization constant. The integrals can be evaluated analytically, leading to

$$k_{5D\rightarrow 5F}(\Delta\omega) = \begin{cases} N\dfrac{c}{2\omega_0 v_0} & \text{for } |\Delta\omega| \leqslant \dfrac{\omega_0 v_0}{c}, \\ 0 & \text{for } |\Delta\omega| > \dfrac{\omega_0 v_0}{c}. \end{cases} \tag{7}$$

$k_{5D\rightarrow 5F}(\Delta\omega)$ describes a "top hat" line shape: constant over a certain region and zero everywhere else. The width of this line shape can be much larger than a typical Doppler-broadened Gaussian line shape associated with a thermalized distribution of atoms. This situation will arise if the translational energy ΔE available after photodissociation satisfies $\Delta E \gg k_{\text{B}}T$ where k_{B} is Boltzmann's constant and T is the absolute temperature.

B. Realistic velocity distribution

We now consider a more sophisticated model for a velocity distribution $f(\mathbf{v})$ that includes the effects of each Cs_2 molecule's internal rovibrational energy and translational energy prior to photodissociation. Henceforth, we will concentrate specifically on the $5D_{3/2}$ atoms produced by molecular photodissociation.

The first effect we consider is that many rovibrational levels in the molecular ground state are thermally populated, and therefore $5D_{3/2}$ atoms with velocities greater than v_0 will be produced by the photodissociation process. As shown in the Appendix, the distribution of thermally populated rovibrational levels of the molecular ground state prior to photodissociation can be modeled by a density of states

$$g(E_{v,J}) = \frac{E_{v,J}}{(k_{\text{B}}T)^2}\exp\left[-\frac{E_{v,J}}{k_{\text{B}}T}\right], \tag{8}$$

where $E_{v,J}$, now regarded as a continuous variable, is the initial rovibrational energy. (Recall $E_{0,0}=0$, so $E_{v,J} \geqslant 0$.) Including the effects of this distribution, but still neglecting the center of mass translational motion of the Cs_2 molecule, we find that the distribution of cesium $5D_{3/2}$ atom velocities after photodissociation is (see the Appendix)

$$f^{(1)}(\mathbf{v}_{\text{ph}}) = \begin{cases} \dfrac{2m^2}{(k_{\text{B}}T)^2}\dfrac{v_{\text{ph}}(v_{\text{ph}}^2 - v_0^2)}{4\pi v_{\text{ph}}^2}\exp\left[-\dfrac{m(v_{\text{ph}}^2 - v_0^2)}{k_{\text{B}}T}\right], & v_{\text{ph}} > v_0 \\ 0, & v_{\text{ph}} \leqslant v_0. \end{cases} \tag{9}$$

The second effect that we consider is that molecules in the vapor have center-of-mass translational velocity before the photodissociation pulse breaks them into separated atoms. This center-of-mass velocity $\mathbf{v}_{\text{c.m.}}$ is passed on to both dissociating atoms and simply adds to the velocity acquired through photodissociation. We can now regard $\mathbf{v}_{\text{ph}}$ as the velocity acquired by the atoms in the rest frame of the Cs_2 molecule; the total velocity of a photodissociated atom in the laboratory frame is

$$\mathbf{v} = \mathbf{v}_{\text{ph}} + \mathbf{v}_{\text{c.m.}}. \tag{10}$$

Prior to photodissociation, the molecules in the vapor have center-of-mass velocities that can be described by a Maxwell-Boltzmann distribution [40]:

$$f^{\text{MB}}_{\text{molecule}}(\mathbf{v}_{\text{c.m.}}) = \left(\frac{M}{2\pi k_{\text{B}}T}\right)^{3/2}\exp\left(-\frac{Mv_{\text{c.m.}}^2}{2k_{\text{B}}T}\right), \tag{11}$$

where $M=2m$ is the mass of the Cs_2 molecule. The final distribution of velocities $f(\mathbf{v})$, characterizing the $5D_{3/2}$ atoms just after they are created by photodissociation, is given by a convolution of the velocity distribution in the rest frame of the parent Cs_2 molecule $f^{(1)}(\mathbf{v}_{\text{ph}})$ with the distribution of Cs_2 center-of-mass velocities:

$$f(\mathbf{v}) = \int f^{(1)}(\mathbf{v} - \mathbf{v}_{\text{c.m.}})f^{\text{MB}}_{\text{molecule}}(\mathbf{v}_{\text{c.m.}})d^3\mathbf{v}_{\text{c.m.}}. \tag{12}$$

The angular parts of this integral may be evaluated analytically, but the rest must be done numerically.

C. Strong-collision model

The velocity distribution derived in Sec. III B [Eq. (12)] applies only in the absence of collisions. Now we consider a simple collision model that includes the effect of thermalizing collisions and that will enable us to interpret the time dependence of our measured line shapes. The key physical point is that collisions gradually change the velocity distribution of excited $5D_{3/2}$ atoms produced by photodissociation [and described by Eq. (12)] to a Maxwell-Boltzmann distribution depending on the temperature. Our time-dependent excitation line shapes allow us to monitor this evolution.

We adopt a very simple Boltzmann equation for the density-velocity distribution $\rho_{5D_{3/2}}(\mathbf{v};t)$ of the $5D_{3/2}$ atoms [41]:

$$\frac{\partial \rho_{5D_{3/2}}(\mathbf{v};t)}{\partial t} = -[\Gamma_{\text{coll}}(\mathbf{v}) + \Gamma_{5D_{3/2}}]\rho_{5D_{3/2}}(\mathbf{v};t) + \int K(\mathbf{v}' \to \mathbf{v})\rho_{5D_{3/2}}(\mathbf{v}';t)d^3\mathbf{v}', \quad (13)$$

where the collision rate $\Gamma_{\text{coll}}(\mathbf{v})$ is determined by the collision kernel K,

$$\Gamma_{\text{coll}}(\mathbf{v}) = \int K(\mathbf{v} \to \mathbf{v}')d^3\mathbf{v}', \quad (14)$$

and $\Gamma_{5D_{3/2}}$ is the total radiative decay rate out of the $5D_{3/2}$ level. We adopt a simple expression for the kernel based on the strong collision model [37,41,42],

$$K(\mathbf{v} \to \mathbf{v}') = \Gamma_{\text{therm}} f_{\text{atom}}^{\text{MB}}(v'), \quad (15)$$

where $f_{\text{atom}}^{\text{MB}}$ is a normalized Maxwellian distribution,

$$f_{\text{atom}}^{\text{MB}}(\mathbf{v}) = \left(\frac{m}{2\pi k_B T}\right)^{3/2} \exp\left(-\frac{mv^2}{2k_B T}\right). \quad (16)$$

The strong-collision model assumes that one single collision is sufficient to thermalize the velocity distribution of the atoms involved. The effective rate of such collisions is given by $\Gamma_{\text{coll}}(\mathbf{v}) = \Gamma_{\text{therm}}$. Even if one physical collision does not totally randomize the velocity, the strong-collision model is often still quite good if $\Gamma_{\text{therm}}^{-1}$ is regarded as the time over which several collisions together effectively randomize the velocity. Substituting the specific form of the kernel K given by Eq. (15) into Eq. (13), we find

$$\frac{\partial \rho_{5D_{3/2}}(\mathbf{v};t)}{\partial t} = -(\Gamma_{\text{therm}} + \Gamma_{5D_{3/2}})\rho_{5D_{3/2}}(\mathbf{v};t) + \Gamma_{\text{therm}} f_{\text{atom}}^{\text{MB}}(\mathbf{v}) n_{5D_{3/2}}(t), \quad (17)$$

where

$$n_{5D_{3/2}}(t) = \int \rho_{5D_{3/2}}(\mathbf{v}';t)d^3\mathbf{v}' \quad (18)$$

is the total density of atoms in the $5D_{3/2}$ level at time t. [Note that according to Ref. [43], the $\text{Cs}(5D_{3/2}) + \text{Cs}(6S_{1/2}) \leftrightarrow \text{Cs}(5D_{5/2}) + \text{Cs}(6S_{1/2})$ collisional excitation transfer rate is smaller than the $5D_{3/2}$ radiative decay rate even at the highest densities used in the present study and much smaller than the thermalization rates measured here. Thus on the time scale of interest for the present experiment, we are justified in neglecting $5D_{3/2} \leftrightarrow 5D_{5/2}$ collisional transfer in Eqs. (13) and (17), especially since the thermalization rates are expected to be comparable for both fine structure levels.] Integrating both sides of Eq. (17) over $\mathbf{v}$ and using Eq. (18) leads to an equation for $n_{5D_{3/2}}(t)$ whose solution is

$$n_{5D_{3/2}}(t) = n_0 \exp(-\Gamma_{5D_{3/2}} t), \quad (19)$$

where n_0 is the initial density of $5D_{3/2}$ atoms just after photodissociation. With this solution for $n_{5D_{3/2}}(t)$, Eq. (17) can be solved exactly:

$$\rho_{5D_{3/2}}(\mathbf{v};t) = \exp(-\Gamma_{5D_{3/2}} t)\{\rho_{5D_{3/2}}(\mathbf{v};0)\exp(-\Gamma_{\text{therm}} t) + n_0[1 - \exp(-\Gamma_{\text{therm}} t)] f_{\text{atom}}^{\text{MB}}(\mathbf{v})\}. \quad (20)$$

This solution has a clear physical interpretation. The leading exponential factor represents the overall radiative decay out of the $5D_{3/2}$ level. The first term inside the braces represents the decay of the initial velocity distribution of $5D_{3/2}$ atoms due to collisions, at the rate Γ_{therm}. The second term shows a corresponding increase in the number of thermalized $5D_{3/2}$ atoms described by the Maxwellian distribution.

We can now identify the term $\rho_{5D_{3/2}}(\mathbf{v};0)$ in Eq. (20) as being proportional to the velocity distribution $f(\mathbf{v})$ [Eq. (12)]. The velocity distribution at $t=0$ characterizes the "fast" $5D_{3/2}$ atoms produced by the photodissociation process. In the strong-collision model analysis, the Maxwellian distribution describes the "slow" atoms that have been thermalized by collisions. We can rewrite Eq. (20) in a way that emphasizes this interpretation:

$$\rho_{5D_{3/2}}(\mathbf{v};t) = n_{5D_{3/2}}^{(\text{fast})}(t) f(\mathbf{v}) + n_{5D_{3/2}}^{(\text{slow})}(t) f_{\text{atom}}^{\text{MB}}(\mathbf{v}), \quad (21)$$

where the "fast" and "slow" atom densities are given by appropriate fractions of the $5D_{3/2}$ atoms that have or have not undergone a thermalizing collision,

$$n_{5D_{3/2}}^{(\text{fast})}(t) = n_{5D_{3/2}}(t)\exp(-\Gamma_{\text{therm}} t) \quad (22)$$

and

$$n_{5D_{3/2}}^{(\text{slow})}(t) = n_{5D_{3/2}}(t)[1 - \exp(-\Gamma_{\text{therm}} t)]. \quad (23)$$

D. Homogeneous line shape

In order to model the $5D_{3/2} \to 5F_{5/2}$ probe-laser-induced excitation line shape, we must convolute the intrinsic homogeneous line shape of the transition with the Doppler shift determined by the component of the atomic velocity in the direction of the laser propagation. Several effects contribute to the homogeneous broadening in the present case. We consider natural (lifetime) broadening, pressure broadening, and optical pumping. We will include these effects in a rate equation model for the density-velocity distributions of the $5D_{3/2}$ and $5F_{5/2}$ levels. The solution to the rate equations, $\rho_{5F_{5/2}}(\mathbf{v}, \Delta\omega; t)$, at various times and various probe laser detunings from the $5D_{3/2} \to 5F_{5/2}$ transition, gives the homogeneous line shape $H(\Delta\omega - \mathbf{k}_L \cdot \mathbf{v}, t)$ for the probe laser excitation scans, because the observed $5F \to 5D_{5/2}$ fluorescence at time t and probe laser detuning $\Delta\omega$ for atoms moving with velocity $\mathbf{v}$ is simply proportional to the density of $5F$ atoms with velocity $\mathbf{v}$ at time t and detuning $\Delta\omega$.

Natural broadening can be described by a Lorentzian function representing each of the hyperfine components of the $5D_{3/2} \to 5F_{5/2}$ transition. For natural broadening, the Lorentzian half width Γ_N is given by

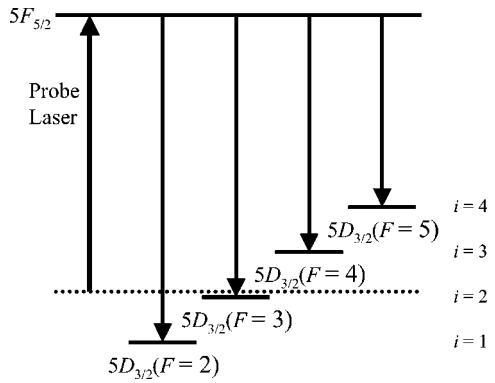

FIG. 4. Energy level diagram used to construct the optical pumping model for the cesium $5D_{3/2} \rightarrow 5F_{5/2}$ transition. The indices $i=1-4$ correspond to the notation used for the $5D_{3/2}$ hyperfine levels in the rate equations given by Eq. (25).

$$\Gamma_N = \sum_j A_{5D_{3/2} \rightarrow j} + \sum_k A_{5F_{5/2} \rightarrow k}, \tag{24}$$

where $A_{i \rightarrow j}$ is the spontaneous emission rate (Einstein A coefficient) for the transition between levels i and j. In the present case, $\Gamma_N = 1.54 \times 10^7\ s^{-1}$ [44].

Pressure broadening due to Cs-Cs collisions can also be represented by a Lorentzian function with a density dependent linewidth, $\Gamma_{br} = k_{br} n_{Cs}$. To the best of our knowledge, the $Cs(5D_{3/2}) \rightarrow Cs(5F_{5/2})$ broadening rate k_{br} has not been determined. However, a crude estimate is $k_{br} \sim 4 \times 10^{-9}\ cm^3\ s^{-1}$ (based on available data for other alkali collisional broadening rates [45–47]). For our range of Cs densities, $n_{Cs} = 3.7 \times 10^{14} - 4.5 \times 10^{15}\ cm^{-3}$, Γ_{br} is likely to be in the range $7 \times 10^5 - 3 \times 10^7\ s^{-1}$, and thus might be significant at our higher densities. However, due to the uncertainty, we decided to neglect Γ_{br} in our homogeneous line shape model. Tests in which we increased $\Gamma_{total} = \Gamma_N + \Gamma_{br}$ by as much as a factor of 2 indicate that neglect of Γ_{br} has little effect on our results. We also ignore $Cs\text{-}Cs_2$ collisions because the molecular density is much lower than the atomic density.

In the present experiment, the intensity of the probe laser is sufficiently high that optical pumping effects are expected. Optical pumping occurs when the laser depletes the population of those lower-state hyperfine levels that possess allowed transitions with which the laser is nearly resonant. Through spontaneous emission, this population is then redistributed among the various hyperfine levels. In the present experiment, the probe laser intensity was $\sim 5\ W/cm^2$ (required to yield acceptable signal to noise) while the saturation intensity of the $5D_{3/2} \rightarrow 5F_{5/2}$ transition is $1.6\ mW/cm^2$ [Eqs. (7.4.5) and (7.5.4) of Ref. [48]].

We now describe the rate equation model that was used to determine the density of upper ($5F_{5/2}$) state atoms, with velocity $\mathbf{v}$. We can write a set of time-dependent rate equations that depends on the quantity $\Delta\omega - \mathbf{k}_L \cdot \mathbf{v}$, which incorporates the effects of the probe laser detuning and the atomic velocity component in the direction of the probe laser propagation. A schematic diagram of the energy levels and transitions is given in Fig. 4. The $5D_{3/2}$ level is made up of four hyperfine levels ($F=2$, 3, 4, 5), which we label as levels $i=1$, 2, 3, 4, respectively. The hyperfine structure of the $5F_{5/2}$ level is neglected, as the level splittings (<10 MHz) are smaller than the homogeneous linewidth. We also take into account the $5F_{5/2} \rightarrow 6D_{3/2,5/2}$ decay channels (in addition to $5F_{5/2} \rightarrow 5D_{3/2,5/2}$) in determining the radiative rate out of the $5F_{5/2}$ level ($\Gamma_{5F_{5/2}} \approx 1.43 \times 10^7\ s^{-1}$) [44]. In the present context, we neglect velocity-changing collisions (these will be incorporated into the model in Sec. IV), as well as collisional excitation transfer to other levels. However, we demonstrate in Ref. [49] that $5D_{3/2} \leftrightarrow 5D_{5/2}$ and $5F_{5/2} \leftrightarrow 5F_{7/2}$ collisional mixings have no significant effect on our measured thermalization rates. Therefore, here we consider an open five-level system with densities dependent on both the probe laser frequency and the time after the pulsed photodissociation laser initially populates the $5D_{3/2}$ level. The rate equations describing the evolution of population in the five levels are

$$\begin{aligned}
&\dot{\rho}_{5F_{5/2}}(\mathbf{v},\Delta\omega;t) \\
&\quad = \sum_{i=1}^{4} P_{i \rightarrow 5F_{5/2}}(\Delta\omega - \mathbf{k}_L \cdot \mathbf{v}) \rho_i(\mathbf{v},\Delta\omega;t) - \Bigg[\Gamma_{5F_{5/2}} \\
&\qquad + \sum_{i=1}^{4} \frac{g_i}{g_{5F_{5/2}}} P_{i \rightarrow 5F_{5/2}}(\Delta\omega - \mathbf{k}_L \cdot \mathbf{v}) \Bigg] \rho_{5F_{5/2}}(\mathbf{v},\Delta\omega;t), \\
&\dot{\rho}_i(\mathbf{v},\Delta\omega;t) \\
&\quad = \Bigg[\Gamma_{5F_{5/2} \rightarrow i} \\
&\qquad + \frac{g_i}{g_{5F_{5/2}}} P_{i \rightarrow 5F_{5/2}}(\Delta\omega - \mathbf{k}_L \cdot \mathbf{v}) \Bigg] \rho_{5F_{5/2}}(\mathbf{v},\Delta\omega;t) \\
&\qquad - [P_{i \rightarrow 5F_{5/2}}(\Delta\omega - \mathbf{k}_L \cdot \mathbf{v}) + \Gamma_{5D_{3/2}}] \rho_i(\mathbf{v},\Delta\omega;t).
\end{aligned} \tag{25}$$

In these equations,

$$P_{i \rightarrow 5F_{5/2}}(\Delta\omega - \mathbf{k}_L \cdot \mathbf{v}) = \frac{B_{i \rightarrow 5F_{5/2}}}{c} I_{laser} L_i(\Delta\omega - \mathbf{k}_L \cdot \mathbf{v}) \tag{26}$$

is the probe laser pumping rate, which enters in both absorption and stimulated emission terms, $B_{i \rightarrow 5F_{5/2}}$ is the Einstein B coefficient, $L_i(\Delta\omega - \mathbf{k}_L \cdot \mathbf{v})$ is the Lorentzian line shape function (due to natural broadening but neglecting pressure broadening, as explained previously) for the $i \rightarrow 5F_{5/2}$ transition evaluated at the Doppler-shifted laser detuning $\Delta\omega - \mathbf{k}_L \cdot \mathbf{v}$, I_{laser} is the laser intensity, and g_i and $g_{5F_{5/2}}$ are statistical weights. The first equation describes the evolution of the $5F_{5/2}$ population for velocity class $\mathbf{v}$, which is proportional to the measured $5F \rightarrow 5D_{5/2}$ fluorescence signal for that velocity class. The second equation describes the evolution of population in each of the four hyperfine levels of the $5D_{3/2}$ state ($i=1-4$)) for this velocity class. The initial conditions are that the density $\rho_{5F_{5/2}}(\mathbf{v},\Delta\omega;t)$ of the upper ($5F_{5/2}$) level is zero at $t=0$ and that the $5D_{3/2}$ hyperfine levels are populated at $t=0$ (by the photodissociation process) in a ratio determined by their statistical weights (5:7:9:11). The

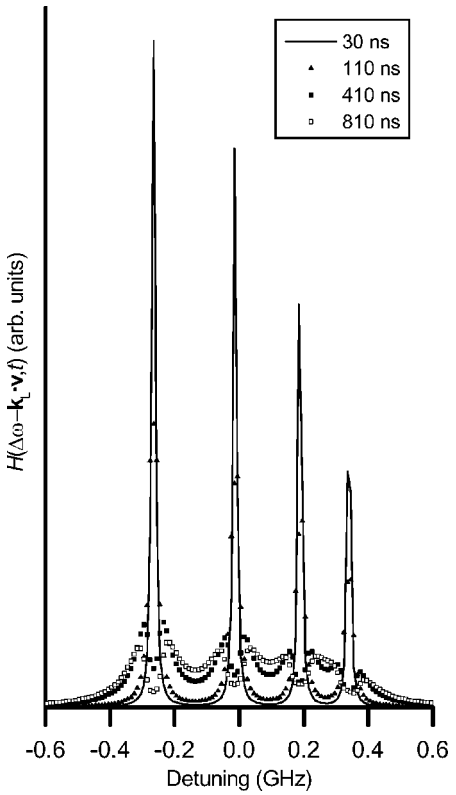

FIG. 5. Homogeneous line shape $H(\Delta\omega-\mathbf{k}_L\cdot\mathbf{v},t)$ obtained from the solution to the optical pumping rate equation model [Eq. (25)] for the time-dependent $5F_{5/2}$ state density-velocity distribution $\rho_{5F_{5/2}}(v,\Delta\omega;t)$ [cf. Eq. (27)].

system of equations was solved numerically as a function of time for each detuning parameter $\Delta\omega-\mathbf{k}_L\cdot\mathbf{v}$ using the MATLAB routine ODE45, which uses a Dormand-Prince (4,5) Runge Kutte formula [50] combined with adaptive step size selection. The calculation was done for each probe laser detuning on a grid of 10 MHz.

For reasons given earlier in this section, we relate the homogeneous line shape function with $\rho_{5F_{5/2}}(\mathbf{v},\Delta\omega;t)$:

$$H(\Delta\omega-\mathbf{k}_L\cdot\mathbf{v},t)\propto\rho_{5F_{5/2}}(\mathbf{v},\Delta\omega;t). \tag{27}$$

The proportionality constant is chosen so that the integral of the homogeneous line shape function $H(\Delta\omega-\mathbf{k}_L\cdot\mathbf{v},t)$ over $\Delta\omega$ is equal to unity.

Figure 5 displays the results of this calculation. The results are shown as a function of detuning for several fixed times. For small but nonzero t, the solution is just the sum of four Lorentzian lines associated with the four hyperfine levels of the $5D_{3/2}$ state, populated in their statistical ratio. As time progresses, optical pumping effects begin to distort the homogeneous line shape. In the late time (a few hundred nanoseconds after the photodissociation pulse) the strong probe laser has severely depleted the population of those hyperfine levels with nearly resonant transitions, creating dips in the line shape at the resonant frequencies of the hyperfine transitions. Additional broadening in the wings of the line is now the prominent feature of the line shape. In the next section, we will convolute this homogeneous line shape with the velocity distribution to model the full probe laser excitation line shape. Because the solution is time dependent, a different homogeneous line shape function must be used to model the data at each time. However, the main contribution of homogeneous broadening occurs in the wings of the line at all times. The overall width of the excitation lines is determined mainly by Doppler broadening.

IV. PREDICTED EXCITATION LINE SHAPE AND FIT TO THE DATA

In the preceding sections, we have considered the effects of the probe-laser-induced optical pumping on the homogeneous line shape (Sec. III D) while neglecting velocity-changing collisions. We have also considered the effects of velocity-changing collisions (in the absence of the probe laser) using the strong collision model (Sec. III C). We are now ready to combine these two models to predict the full excitation line shapes.

The contribution to the probe laser induced fluorescence (excitation) line shape for an atom moving with velocity $\mathbf{v}$ is proportional to the Doppler shifted homogeneous line shape determined in Sec. III D. For a sample of $5D_{3/2}$ atoms characterized by density-velocity distribution $\rho_{5D_{3/2}}(\mathbf{v};t)$, the line shape (normalized $5F\rightarrow5D_{5/2}$ fluorescence intensity as a function of probe laser detuning near the $5D_{3/2}\rightarrow5F_{5/2}$ transition at time t) is given by the convolution

$$I_{5F\rightarrow5D_{5/2}}(\Delta\omega,t)=\frac{1}{n_{5D_{3/2}}(t)}\int H(\Delta\omega-\mathbf{k}_L\cdot\mathbf{v},t)\rho_{5D_{3/2}}(\mathbf{v};t)d^3\mathbf{v}. \tag{28}$$

Substituting the form of $\rho_{5D_{3/2}}(\mathbf{v};t)$ determined in Eqs. (21)–(23) leads to

$$\begin{aligned}I_{5F\rightarrow5D_{5/2}}(\Delta\omega,t)&=\frac{n^{(\mathrm{fast})}_{5D_{3/2}}(t)}{n_{5D_{3/2}}(t)}I^{(\mathrm{fast})}_{5F\rightarrow5D_{5/2}}(\Delta\omega,t)+\frac{n^{(\mathrm{slow})}_{5D_{3/2}}(t)}{n_{5D_{3/2}}(t)}I^{(\mathrm{slow})}_{5F\rightarrow5D_{5/2}}(\Delta\omega,t)\\&=\exp(-\Gamma_{\mathrm{therm}}t)I^{(\mathrm{fast})}_{5F\rightarrow5D_{5/2}}(\Delta\omega,t)\\&\quad+[1-\exp(-\Gamma_{\mathrm{therm}}t)]I^{(\mathrm{slow})}_{5F\rightarrow5D_{5/2}}(\Delta\omega,t),\end{aligned} \tag{29}$$

where we have defined separate contributions from the "fast" and "slow" components of our model velocity distribution:

$$I^{(\mathrm{fast})}_{5F\rightarrow5D_{5/2}}(\Delta\omega,t)=\int H(\Delta\omega-\mathbf{k}_L\cdot\mathbf{v},t)f(\mathbf{v})d^3\mathbf{v} \tag{30}$$

and

$$I^{(\mathrm{slow})}_{5F\rightarrow5D_{5/2}}(\Delta\omega,t)=\int H(\Delta\omega-\mathbf{k}_L\cdot\mathbf{v},t)f^{\mathrm{MB}}_{\mathrm{atom}}(\mathbf{v})d^3\mathbf{v}. \tag{31}$$

Note that the homogeneous line shape $H(\Delta\omega-\mathbf{k}_L\cdot\mathbf{v},t)$ is time dependent, due to the optical pumping effects, so both fast and slow line shapes have a small dependence on time. For each time of interest, one must calculate a fast and a slow atom line shape. The calculation is performed numerically. $H(\Delta\omega-\mathbf{k}_L\cdot\mathbf{v},t)$ is determined from the solution to the

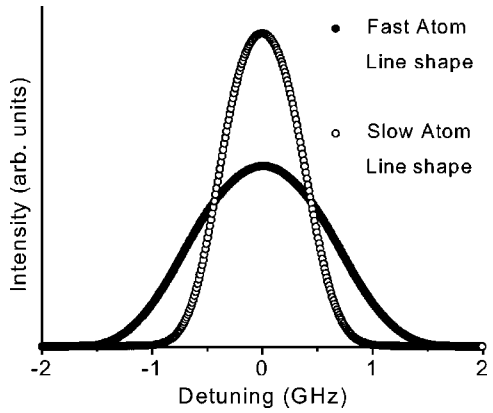

FIG. 6. Fast (●) and slow (○) atom line shape functions [defined in Eqs. (30) and (31)] computed for a delay time of 30 ns after the photodissociation pulse and a cell temperature of 208 °C ($n_{\mathrm{Cs}}=2.41\times10^{15}$ cm^{-3}). The line shapes have been normalized to have the same area.

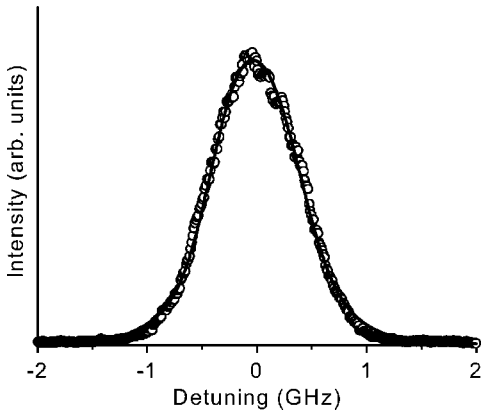

FIG. 7. Fit of one $5D_{3/2}\rightarrow5F_{5/2}$ excitation line shape, recorded at a delay time of 300 ns, to a linear combination of fast and slow atom line shapes. The fitting parameters for this data set are $B=88.9$, $C=0.146$, and $\Gamma_{\mathrm{therm}}=3.73\times10^{6}$ s^{-1}. The frequency scale was adjusted by 0.096 GHz, in order to match line center. The cell temperature for this data set was $T=208$ °C and $n_{\mathrm{Cs}}=2.41\times10^{15}$ cm^{-3}. The experimental points are represented by open circles (○) and the solid curve is the fit.

rate equations [Eq. (25)] as described earlier; $f(\mathbf{v})$ is determined by numerical integration [Eqs. (9)–(12)], and $f_{\mathrm{atom}}^{\mathrm{MB}}(\mathbf{v})$ is known analytically [Eq. (16)]. The line center ($\omega=\omega_0$) is taken as the weighted average of the four $5D_{3/2}(F)\rightarrow5F_{5/2}$ hyperfine transitions [51]. The line shapes $I_{5F\rightarrow5D_{5/2}}^{(\mathrm{fast})}$ and $I_{5F\rightarrow5D_{5/2}}^{(\mathrm{slow})}$ are separately normalized so that their integrals over detuning are unity.

Figure 6 shows examples of these line shapes. The fast atom line shape is broad because of the Doppler shifts associated with high speeds and is slightly asymmetric due to shifted centers and weightings of the four hyperfine components. The slow (thermal) atom line shape more closely resembles a Voigt profile, but is somewhat different because the homogeneous line shape is not a pure Lorentzian, even in the earliest times.

We fit our data at each delay time to a linear combination of fast and slow atom line shapes [Eq. (29)]. The explicit form of the fitting function we used is

$$\begin{aligned} I_{5F\rightarrow5D_{5/2}}(\omega-\omega_0,t) &= B\{\exp(-\Gamma_{\mathrm{therm}}t)I_{5F\rightarrow5D_{5/2}}^{(\mathrm{fast})}(\omega-\omega_0,t) \\ &\quad+[1-\exp(-\Gamma_{\mathrm{therm}}t)]I_{5F\rightarrow5D_{5/2}}^{(\mathrm{slow})}(\omega-\omega_0,t)\}+C. \end{aligned} \tag{32}$$

In this expression, B is the overall normalization factor (taking into account detector efficiency, etc.) and C is a base line correction that takes into account the nonzero voltage offset of the boxcar averager. Neither of these fitting parameters is significant in determining the thermalization rate, but must be allowed to vary in order to obtain satisfactory fits of the data and accurate values for Γ_{therm}. The line center frequency ω_0 is also allowed to vary to compensate for small absolute errors in the probe laser wavemeter readings.

A typical scan with fitted line shape is shown in Fig. 7. For a given data set, we input the known delay time between the end of the photodissociation laser pulse and the center of the fluorescence collection window, and fit the data with the four parameters (B, C, ω_0, and Γ_{therm}), using a general least-squares fitting program [52]. Data were taken at several delay times for a given Cs ground-state density. A plot of Γ_{therm} as a function of time for $T=208$ °C ($n_{\mathrm{Cs}}=2.41\times10^{15}$ cm^{-3}) is shown in Fig. 8. The strong-collision model predicts that Γ_{therm} should be a constant in time and this appears to be true within experimental uncertainties.

For each Cs ground-state density, a best value of Γ_{therm} was determined from a weighted average of all scans and delay times recorded at that density. We note that very early

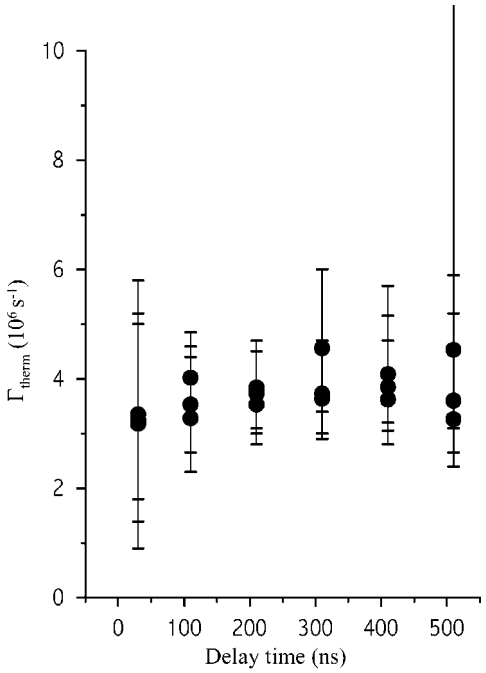

FIG. 8. Plot of Γ_{therm} (obtained from the strong collision model fit of the data) vs time after the photodissociation laser pulse at $T=208$ °C and $n_{\mathrm{Cs}}=2.41\times10^{15}$ cm^{-3}.

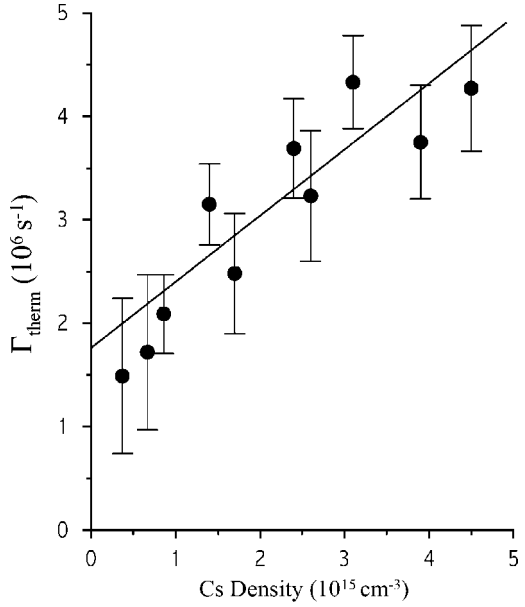

FIG. 9. Plot of Γ_{therm} vs Cs density. The solid line represents the best straight line fit to the data, and its slope gives the value of the velocity-changing collision rate coefficient, $k_{\text{VCC}}^{\text{Cs}} = (6.1 \pm 1.2) \times 10^{-10}$ cm^3 s^{-1}.

time and very late time delays have large error bars due to the fact that the observed line shapes are almost pure "fast" or pure "slow" atom line shapes in those limits and therefore they are not sensitive to the value of Γ_{therm}.

A plot of Γ_{therm} versus cesium ground-state density is shown in Fig. 9. The error bars represent the standard deviation of the averaged Γ_{therm} values for all data taken at a given density. If the observed thermalization of $\text{Cs}(5D_{3/2})$ atoms was due only to collisions with ground-state cesium atoms, we would expect

$$\Gamma_{\text{therm}} = k_{\text{VCC}} n_{\text{Cs}} = \langle \sigma_{\text{VCC}} v \rangle n_{\text{Cs}} \equiv \sigma_{\text{VCC}}^{\text{eff}} \langle v \rangle n_{\text{Cs}}, \qquad (33)$$

where k_{VCC} and $\sigma_{\text{VCC}}^{\text{eff}}$ are the velocity-changing collision rate coefficient and the velocity-averaged (effective) cross section, respectively, and $\langle v \rangle$ is the average collision speed (which is approximately equal to the speed of the excited atom created in the photodissociation process). Our data do show this linear relationship. However, the nonzero intercept implies that thermalization also occurs through collisions with impurity gases in the sealed cesium cell. Thus we fit the thermalization rate versus Cs density with the function

$$\Gamma_{\text{therm}} = k_{\text{VCC}}^{\text{Cs}} n_{\text{Cs}} + k_{\text{VCC}}^{\text{Im}} n_{\text{Im}} = k_{\text{VCC}}^{\text{Cs}} n_{\text{Cs}} + \text{const}, \qquad (34)$$

where we assume that the impurity contribution $k_{\text{VCC}}^{\text{Im}} n_{\text{Im}}$ is constant in temperature. We do not know much about the nature or concentration of the impurities in our cell, so we do not try to determine $k_{\text{VCC}}^{\text{Im}}$. However, we have also observed the effects of the impurities in the same cell in studies of the fine structure changing collision process, $\text{Cs}(6P_{3/2}) + X \rightarrow \text{Cs}(6P_{1/2}) + X$, where X is the impurity collision partner [49].

The slope of the best-fit line yields the cesium velocity-changing collision rate coefficient,

$$k_{\text{VCC}}^{\text{Cs}} = (6.1 \pm 1.2) \times 10^{-10} \text{ cm}^3 \text{ s}^{-1}, \qquad (35)$$

while the effective cross section is

$$\sigma_{\text{VCC}}^{\text{Cs,eff}} = (1.2 \pm 0.2) \times 10^{-14} \text{ cm}^2. \qquad (36)$$

The error bars given in Eqs. (35) and (36) are the statistical errors only. In Ref. [49], we examine the effects of the nonzero $5F_J$ state lifetimes and the nonzero duration of the boxcar averager fluorescence collection window on the experimental values for Γ_{therm}. In that reference, we solve the coupled-state rate equations in the weak and strong pumping limits and show that the errors in our measured thermalization rates due to these effects are less than 50% in the worst case (large Γ_{therm}, early time, weak pumping limit) and are typically less than 20%. Roughly speaking, averaging over the 20-ns boxcar gate duration is found to have little effect on the measured thermalization times, which range between 200 ns and 1 μs. The nonzero $5F_J$ state lifetimes ($\sim$70 ns) are more significant because they introduce a systematic error into the results. Although our recorded signal is the $5F \rightarrow 5D_{5/2}$ fluorescence observed at time t, the sensitivity of the probe laser technique to fast versus slow atoms occurs at the point of absorption (which, in general, is earlier than t due to the nonzero $5F_J$ state lifetimes), rather than at the point of emission. In the weak pumping limit (weak probe laser limit), we find that this effect does not depend strongly on the value of Γ_{therm} (for the range of Γ_{therm} values used in this work), but does depend strongly on the observation time. However, if we instead use a strong pumping model (which should be more applicable for the present experiment), then this effect is dramatically reduced as the effective upper-state lifetime is decreased due to stimulated emission. In this latter case, light-induced drift effects could be included by assigning different thermalization rates to the $5D_{3/2}$ and $5F_{5/2}$ levels [37], but this would represent a higher-order correction to the rate equations. Thus we conclude that the systematic errors in $k_{\text{VCC}}^{\text{Cs}}$ and $\sigma_{\text{VCC}}^{\text{Cs,eff}}$, which are determined from an average over many Γ_{therm} values obtained at different observation times and densities, are probably no more than 20%.

V. ELECTRONIC STATES RESPONSIBLE FOR THE OBSERVED PHOTODISSOCIATION OF Cs_2

This section addresses the question of which electronic states of Cs_2 are responsible for the photodissociation process observed in this work. Our analysis draws on the theoretical potential curves of Spies [53], the selection rules for predissociation and photodissociation [39], and the experiments of Collins *et al.* [2]. Because Collins *et al.* [2] noticed that the blue Cs_2 photolysis band they observed closely resembled the shape of the $E \leftarrow X$ absorption band, they suggested that the photolysis most likely occurred through predissociation of the bound $E\ ^1\Pi_u$ state by the repulsive limb of the $3\ ^3\Sigma_u^+$ state. Conversely, they attributed the green Cs_2 photolysis band (which also produces $5D + 6S$ atoms) to direct dissociation to the $2\ ^1\Sigma_u^+$ state. It is now known that there are two upper states associated with the $E \leftarrow X$ absorption band: $3\ ^1\Sigma_u^+$ (dissociating to the $7S + 6S$ limit) and $3\ ^1\Pi_u$ (dissociating to the $7P + 6S$ limit) [54–56]. Figure 10(a) shows

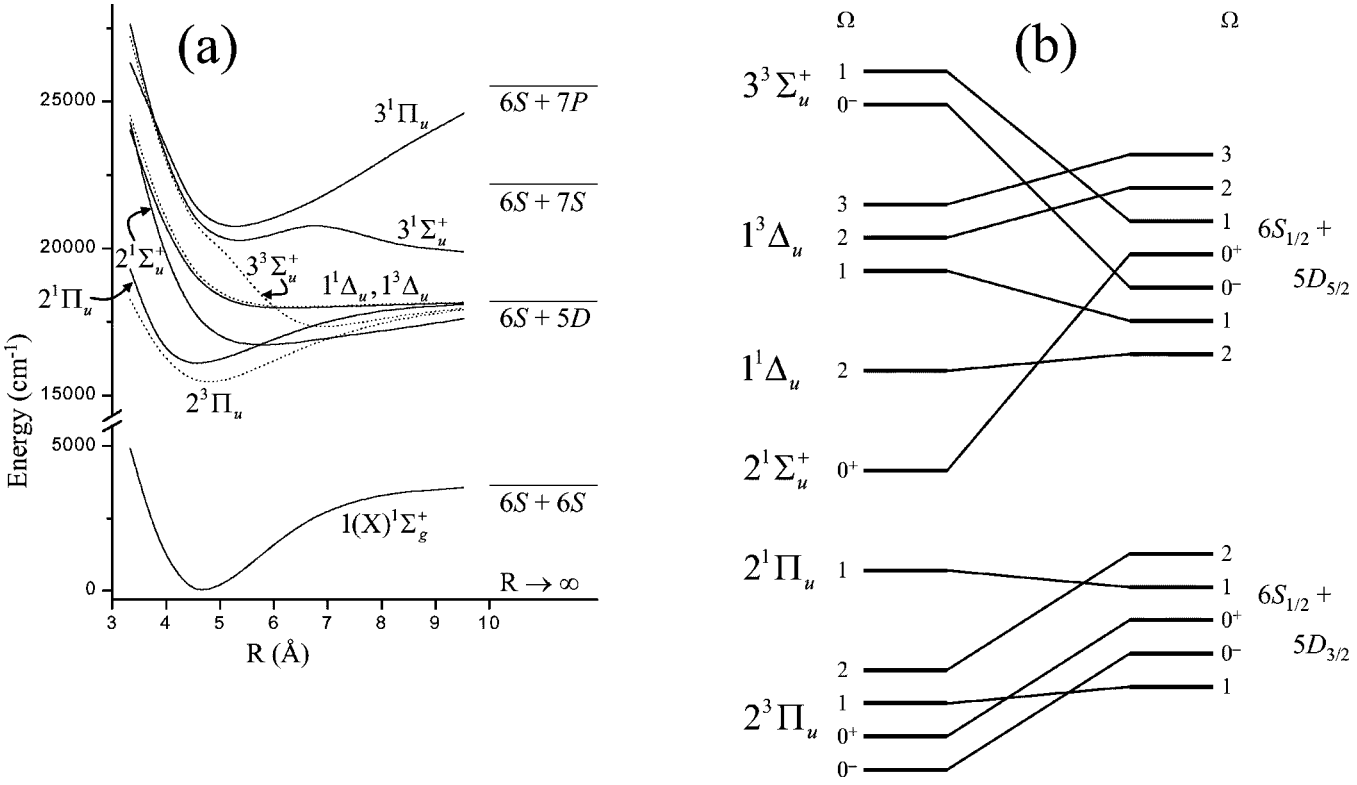

FIG. 10. (a) Selected Cs_2 potential energy curves from Ref. [53]. Solid lines represent singlet states while dotted lines represent triplet states. (b) Correlation diagram showing the adiabatic coupling between the Hund's case (a) molecular states at the ground-state equilibrium separation $R=4.66$ Å and the Hund's case (c) separated atom limits.

selected theoretical potentials from Ref. [53]. Only excited *ungerade* states are accessible with single-photon excitation from the ground state. From the diagram, it appears that the predissociation mechanism suggested by Collins *et al.* [2] is quite plausible. We calculated rates for this process using the computer code BCONT [57] and the potentials of Ref. [53]. The original *ab initio* potentials led to rather small predissociation rates ($\lesssim 10^3$ s^{-1}). However, slightly modified potentials yielded much larger rates. Shifting the $3\,^3\Sigma_u^+$ potential curve upward in energy by $\sim$500 cm^{-1} or shifting it to larger internuclear separations by $\sim$0.16 Å produced predissociation rates greater than 10^8 s^{-1}.

The other possible mechanism is direct excitation to the continuum of one of the various *ungerade* states dissociating to the $5D+6S$ atomic limit. Of these six possible *ungerade* states, we can immediately eliminate the $2\,^1\Sigma_u^+$, $2\,^1\Pi_u$, and $2\,^3\Pi_u$ states because absorption from the ground state to these states does not occur in the blue part of the spectrum [7–12,58,59]. The $1\,^1\Delta_u$ state cannot be reached from the ground state $X\,^1\Sigma_g^+$ due to the $\Delta\Omega=0,\pm1$ selection rule. Transitions from the ground state to the $1\,^3\Delta_u$ state $\Omega=1$ component are allowed by the $\Delta\Omega$ selection rule, but are still forbidden by the $\Delta\Lambda=0,\pm1$ and $\Delta S=0$ selection rules (although neither Λ nor S is a good quantum number for the heavy Cs_2 molecule).

We also calculated direct bound-free absorption spectra involving the $3\,^3\Sigma_u^+$ and $2\,^1\Sigma_u^+$ states using BCONT [57] and the theoretical potentials of Ref. [53]. We found that the bound-free part of the $2\,^1\Sigma_u^+\leftarrow X\,^1\Sigma_g^+$ absorption peaks in the green part of the spectrum, as Collins *et al.* [2] suggested, while the $3\,^3\Sigma_u^+\leftarrow X\,^1\Sigma_g^+$ bound-free absorption peaks in the blue. Figure 10(b) shows a correlation diagram for the states dissociating to the $5D+6S$ atomic limit, where it can be seen that both the $2\,^1\Sigma_u^+$ and $3\,^3\Sigma_u^+$ states dissociate adiabatically to the $5D_{5/2}+6S_{1/2}$ limit. This behavior appears to be inconsistent with the observation of Collins *et al.* [2] that the $5D_{3/2}$ atomic level is approximately 1.8 times more likely to be populated than the $5D_{5/2}$ level by blue light photolysis of Cs_2. However, we note that the $3\,^3\Sigma_u^+$ state crosses the $2\,^1\Pi_u$ state at intermediate R [see Fig. 10(a)], and the $\Omega=1$ components of these states are expected to couple through the spin-orbit interaction. Thus the doubly degenerate $\Omega=1$ component of $3\,^3\Sigma_u^+$ is likely to dissociate diabatically to the $5D_{3/2}+6S_{1/2}$ limit, while the singly degenerate $\Omega=0^-$ is likely to dissociate to the $5D_{5/2}+6S_{1/2}$ limit. Similarly, Collins *et al.* [2] found that $5D_{5/2}$ was approximately 2.8 times as likely to be populated as $5D_{3/2}$ in the green photolysis band. The $2\,^1\Sigma_u^+$ state dissociates adiabatically to the $5D_{5/2}+6S_{1/2}$ limit. But it crosses the $2\,^3\Pi_u$ state (which dissociates to the $5D_{3/2}$ limit) at intermediate internuclear separation and the $\Omega=0^+$ components of these states should also couple through the spin-orbit interaction.

We conclude that the photodissociation of Cs_2 molecules with blue light studied in the present work most likely occurs through direct excitation of the $3\,^3\Sigma_u^+$ state or by predissociation of the bound $3\,^1\Pi_u$ state by $3\,^3\Sigma_u^+$. This conclusion is consistent with the results and analysis of Collins *et al.* [2].

VI. CONCLUDING REMARKS

We have studied the thermalization of fast, excited cesium atoms by collisions with slow ground-state atoms. The reaction process can be described by

$$\mathrm{Cs}(5D_{3/2})_{\mathrm{fast}} + \mathrm{Cs}(6S_{1/2}) \rightarrow \mathrm{Cs}(5D_{3/2})_{\mathrm{slow}} + \mathrm{Cs}(6S_{1/2}). \tag{37}$$

This velocity-changing collision process is different from the resonance exchange process studied by Huennekens *et al.* [60] and Kaufmann *et al.* [61] where atom trajectories are not necessarily altered, but excitation is transferred through the exchange of a virtual or real photon. Calculated resonance exchange cross sections are very large, greater than 10^{-12} cm^2 [60–62]. However, the resonance exchange process is not significant in the present case because the $5D \rightarrow 6S$ transition is dipole forbidden and the resonance exchange cross section should, therefore, be several orders of magnitude smaller. There might still be resonance exchange collisions of Cs($5D$) and Cs($6P$) atoms, but the density of the latter species is five orders of magnitude lower than the ground-state density, so this process can also be neglected. The velocity-changing collision cross section we obtain in the present work is $\sim 10^{-14}$ cm^2 and is consistent with other previously measured velocity-changing collision cross sections [17,21,25].

As discussed in Sec. III C, the experimental data reported here were analyzed using the strong collision model. Unfortunately, the time dependence of the measured excitation line shapes is not sufficiently large to justify a detailed comparison of the strong-collision model with more sophisticated collision kernels. Nonetheless, the present work demonstrates that photodissociation can produce excited atoms with well-defined speeds that are much greater than those found in a thermal vapor and that can be controlled with the photodissociation laser wavelength. The thermalization of these fast, excited atoms through velocity-changing collisions is the first collision process we have studied using this unique velocity-selected source. In this first project we have only looked at one range of initial velocities ($v \geqslant v_0 = 5.1 \times 10^4$ cm/s) corresponding to a photodissociation wavelength of 475.8 nm. In future work we plan to vary the initial velocity systematically by changing the photodissociation laser wavelength. We also plan to use state-selective techniques to improve the velocity resolution. Another possible experiment is to look for anisotropic velocity distributions from photodissociation with polarized light by using a spatially displaced probe beam and comparing results for different polarizations of the photodissociation laser. We believe that it is possible to use the basic technique outlined in this paper to study the velocity dependence of a wide variety of atomic collision processes involving excited atoms, and this is the direction of our future work.

ACKNOWLEDGMENTS

The authors would like to thank Professor H. Katô for providing a copy of the theoretical Cs_2 potentials of Spies. This work was supported by NSF Grant No. PHY-0244767. A.M. was partially supported by the U.S. Department of Education through the GAANN program.

APPENDIX: EFFECT OF THE THERMAL DISTRIBUTION OF POPULATION OVER ROVIBRATIONAL LEVELS OF THE MOLECULAR GROUND STATE ON THE "FAST" EXCITED-ATOM VELOCITY DISTRIBUTION AFTER PHOTODISSOCIATION

To consider this effect on the "fast" excited-atom velocity distribution, we start by assuming that the initial population of molecular ground-state (v, J) levels follows a thermal distribution:

$$N(v,J) \propto (2J+1)\exp\left[-\frac{E_{v,J}}{k_{\mathrm{B}}T}\right]. \tag{A1}$$

Because a great number of rovibrational levels are thermally populated, we may treat $E_{v,J}$ as a continuous variable. We can approximate the molecular energy (referenced to $E_{0,0}$) as

$$E_{v,J} = \omega_{\mathrm{e}} v + B_{\mathrm{e}} J(J+1), \tag{A2}$$

where ω_{e} and B_{e} are the vibrational and rotational constants.

For the $v=0$ level, the density of rotational levels with energies between E and $E+dE$ is proportional to the number of levels between J and $J+dJ$, where $dJ=(dJ/dE)dE$:

$$\begin{aligned} g_{v=0}(E)dE \propto N(v=0,J)dJ = N(v=0,J)\left(\frac{dE}{dJ}\right)^{-1} dE \\ \propto \frac{(2J+1)\exp\left[-\dfrac{B_{\mathrm{e}}J(J+1)}{k_{\mathrm{B}}T}\right]}{(2J+1)B_{\mathrm{e}}} dE \\ = \frac{\exp\left[-\dfrac{E}{k_{\mathrm{B}}T}\right]}{B_{\mathrm{e}}} dE. \end{aligned} \tag{A3}$$

This is the only vibrational level that contributes for $E_{0,0} < E < E_{1,0}$. Similarly, for $v=1$,

$$\begin{aligned} g_{v=1}(E)dE \propto \frac{(2J+1)\exp\left[-\dfrac{\omega_{\mathrm{e}} + B_{\mathrm{e}}J(J+1)}{k_{\mathrm{B}}T}\right]}{(2J+1)B_{\mathrm{e}}} d\mathrm{E} \\ = \frac{\exp\left[-\dfrac{E}{k_{\mathrm{B}}T}\right]}{B_{\mathrm{e}}} dE. \end{aligned} \tag{A4}$$

We can generalize this to include all vibrational levels with $E_{v,J=0} < E$ and sum over all levels to obtain

$$g(E)dE \propto \sum_{v=0}^{v_{\max}} \frac{\exp\left[-\dfrac{E}{k_{\mathrm{B}}T}\right]}{B_{\mathrm{e}}} dE = (v_{\max}+1)\frac{\exp\left[-\dfrac{E}{k_{\mathrm{B}}T}\right]}{B_{\mathrm{e}}} dE. \tag{A5}$$

Here $v_{\max}$ is determined from

$$E_{v_{\max},J=0} < E < E_{v_{\max}+1,J=0}, \tag{A6}$$

which yields

$$v_{\max} < \frac{E}{\omega_e} < v_{\max} + 1. \tag{A7}$$

Thus we can write $(v_{\max}+1) \approx E/\omega_e$. The resulting density of states is therefore given by

$$g(E)dE \propto \frac{E}{\omega_e B_e} \exp\left[-\frac{E}{k_B T}\right] dE, \tag{A8}$$

and normalization yields the final result

$$g(E)dE = \frac{E}{(k_B T)^2} \exp\left[-\frac{E}{k_B T}\right] dE. \tag{A9}$$

The speed of an excited $5D$ atom just after it is created through the photodissociation of a molecule initially occupying level v, J of the ground state is obtained from the relation

$$m v_{\rm ph}^2 = \Delta E = (\hbar\omega_{\rm pump} - E_{5D+6S}) + E_{v,J} = m v_0^2 + E_{v,J}, \tag{A10}$$

where again, all energies are referenced to the $v=0$, $J=0$ energy level of the molecular ground state. We can therefore express the molecular rovibrational energy as a function of atomic velocity:

$$E_{v,J} = m(v_{\rm ph}^2 - v_0^2). \tag{A11}$$

Thus the probability of finding excited $5D$ atoms with velocities between $\mathbf{v}_{\rm ph}$ and $\mathbf{v}_{\rm ph} + d^3\mathbf{v}_{\rm ph}$ after photodissociation is equal to the probability of finding ground-state molecules with rovibrational energies between E and $E+dE$ prior to photodissociation,

$$f^{(1)}(\mathbf{v}_{\rm ph}) d^3\mathbf{v}_{\rm ph} = f^{(1)}(v_{\rm ph}) 4\pi v_{\rm ph}^2 dv_{\rm ph} = g(E)dE, \tag{A12}$$

where we assume that the velocity distribution is isotropic. (Note that the polarized photodissociation laser pulse may produce an anisotropic velocity distribution. In future work we plan to use a spatially displaced probe beam to study this effect—see Sec. VI.) Using Eq. (A9) for the density of states we find

$$f^{(1)}(\mathbf{v}_{\rm ph}) d^3\mathbf{v}_{\rm ph} = \frac{g(E)}{4\pi v_{\rm ph}^2} \frac{dE}{dv_{\rm ph}} d^3\mathbf{v}_{\rm ph} = \begin{cases} \dfrac{2m^2}{(k_B T)^2} \dfrac{v_{\rm ph}(v_{\rm ph}^2 - v_0^2)}{4\pi v_{\rm ph}^2} \exp\left[\dfrac{-m(v_{\rm ph}^2 - v_0^2)}{k_B T}\right] d^3\mathbf{v}_{\rm ph} & \text{for } v_{\rm ph} > v_0, \\ 0 & \text{for } v_{\rm ph} \leqslant v_0. \end{cases} \tag{A13}$$

[1] C. B. Collins, J. A. Anderson, F. W. Lee, P. A. Vicharelli, D. Popescu, and I. Popescu, Phys. Rev. Lett. **44**, 139 (1980).
[2] C. B. Collins, J. A. Anderson, D. Popescu, and I. Popescu, J. Chem. Phys. **74**, 1053 (1981).
[3] C. B. Collins, F. W. Lee, J. A. Anderson, P. A. Vicharelli, D. Popescu, and I. Popescu, J. Chem. Phys. **74**, 1067 (1981).
[4] C. B. Collins, F. W. Lee, H. Golnabi, F. Davanloo, P. A. Vicharelli, D. Popescu, and I. Popescu, J. Chem. Phys. **75**, 4852 (1981).
[5] F. Davanloo, F. W. Lee, and C. B. Collins, J. Chem. Phys. **77**, 5455 (1982).
[6] F. Davanloo, C. B. Collins, A. S. Inamdar, N. Y. Mehendale, and A. S. Naqvi, J. Chem. Phys. **82**, 4965 (1985).
[7] M. Baba, T. Nakahori, T. Iida, and H. Katô, J. Chem. Phys. **93**, 4637 (1990).
[8] H. Katô, T. Kobayashi, M. Chosa, T. Nakahori, T. Iida, S. Kasahara, and M. Baba, J. Chem. Phys. **94**, 2600 (1991).
[9] T. Kobayashi, T. Usui, T. Kumauchi, M. Baba, K. Ishikawa, and H. Katô, J. Chem. Phys. **98**, 2670 (1993).
[10] S. Kasahara, Y. Hasui, K. Otsuka, M. Baba, W. Demtröder, and H. Katô, J. Chem. Phys. **106**, 4869 (1997).
[11] S. Kasahara, K. Otsuka, M. Baba, and H. Katô, J. Chem. Phys. **109**, 3393 (1998).
[12] Y. Kimura, H. Lefebvre-Brion, S. Kasahara, H. Katô, M. Baba, and R. Lefebvre, J. Chem. Phys. **113**, 8637 (2000).
[13] R. Schmiedl, H. Dugan, W. Meier, and K. H. Welge, Z. Phys. A **304**, 137 (1982).
[14] R. Vasudev, R. N. Zare, and R. N. Dixon, J. Chem. Phys. **80**, 4863 (1984).
[15] S. Klee, K.-H. Gericke, and F. J. Comes, J. Chem. Phys. **85**, 40 (1986).
[16] Z. Xu, B. Koplitz, and C. Wittig, J. Chem. Phys. **90**, 2692 (1989).
[17] G. Nan and P. L. Houston, J. Chem. Phys. **97**, 7865 (1992).
[18] S. W. North, X. S. Zheng, R. Fei, and G. E. Hall, J. Chem. Phys. **104**, 2129 (1996).
[19] M. Borenstein and W. E. Lamb, Jr., Phys. Rev. A **5**, 1311 (1972).
[20] J. Apt and D. E. Pritchard, Phys. Rev. Lett. **37**, 91 (1976).
[21] P. F. Liao, J. E. Bjorkholm, and P. R. Berman, Phys. Rev. A **21**, 1927 (1980).
[22] H. M. Pickett, J. Chem. Phys. **73**, 6090 (1980).
[23] W. A. Hamel, J. E. M. Haverkort, H. G. C. Werij, and J. P. Woerdman, J. Phys. B **19**, 4127 (1986).
[24] G. Nienhuis and S. Kryszewski, Phys. Rev. A **36**, 1305 (1987).
[25] J. E. M. Haverkort, J. P. Woerdman, and P. R. Berman, Phys. Rev. A **36**, 5251 (1987).
[26] H. G. C. Werij and J. P. Woerdman, Phys. Rep. **169**, 145 (1988).
[27] M. J. O'Callaghan, and A. Gallagher, Phys. Rev. A **39**, 6190

(1989).
[28] M. J. O'Callaghan, and J. Cooper, Phys. Rev. A **39**, 6206 (1989).
[29] K. E. Gibble and A. Gallagher, Phys. Rev. A **43**, 1366 (1991).
[30] K. E. Gibble and J. Cooper, Phys. Rev. A **44**, R5335 (1991).
[31] K. E. Gibble and J. Cooper, Phys. Rev. Lett. **67**, 1936 (1991).
[32] G. Shimkaveg, W. W. Quivers, Jr., R. R. Dasari, and M. S. Feld, Phys. Rev. A **48**, 1409 (1993).
[33] R. K. Namiotka, E. Ehrlacher, J. Sagle, M. Brewer, D. J. Namiotka, A. P. Hickman, A. D. Streater, and J. Huennekens, Phys. Rev. A **54**, 449 (1996).
[34] R. Ciurylo, D. Lisak, and J. Szudy, Phys. Rev. A **66**, 032701 (2002).
[35] Y. Ohta, M. Hasuo, and T. Fujimoto, Opt. Commun. **210**, 245 (2002).
[36] E. Ehrlacher, Ph.D. thesis, Lehigh University, 1993.
[37] A. D. Streater and J. P. Woerdman, J. Phys. B **22**, 677 (1989).
[38] A. N. Nesmeyanov, *Vapour Pressure of the Elements* (Academic Press, New York, 1963).
[39] G. Herzberg, *Molecular Spectra and Molecular Structure I: Spectra of Diatomic Molecules* (Krieger, Malabar, 1989).
[40] F. Reif, *Fundamentals of Statistical and Thermal Physics* (McGraw-Hill, New York, 1965).
[41] P. R. Berman, J. E. M. Haverkort, and J. P. Woerdman, Phys. Rev. A **34**, 4647 (1986).
[42] J. Keilson and K. E. Storer, Q. Appl. Math. **10**, 243 (1952).
[43] A. Sasso, W. Demtröder, T. Colbert, C. Wang, E. Ehrlacher, and J. Huennekens, Phys. Rev. A **45**, 1670 (1992).
[44] B. Warner, Mon. Not. R. Astron. Soc. **139**, 115 (1968).
[45] R. H. Chatham, A. Gallagher, and E. L. Lewis, J. Phys. B **13**, L7 (1980).
[46] J. F. Kielkopf, J. Phys. B **13**, 3813 (1980).
[47] M. V. Romalis, E. Miron, and G. D. Cates, Phys. Rev. A **56**, 4569 (1997).
[48] P. W. Milonni and J. H. Eberly, *Lasers* (Wiley, New York, 1988).
[49] A. Marks, Ph.D. thesis, Lehigh University, 2004.
[50] J. R. Dormand and P. J. Prince, J. Comput. Appl. Math. **6**, 19 (1980).
[51] E. Arimondo, M. Inguscio, and P. Violino, Rev. Mod. Phys. **49**, 31 (1977).
[52] B. S. Garbow, K. E. Hillstrom, and J. J. More, subroutines LMDIF and LMDIF1 from the minpack library, available from http://www.netlib.org (1980).
[53] N. Spies, Ph.D. thesis, Universität Kaiserslautern, 1989.
[54] C. Amiot, C. Crépin, and J. Vergès, J. Mol. Spectrosc. **107**, 28 (1984).
[55] C. Amiot, W. Demtröder, and C. R. Vidal, J. Chem. Phys. **88**, 5265 (1988).
[56] C. Amiot, J. Chem. Phys. **89**, 3993 (1988).
[57] R. J. LeRoy and G. T. Kraemer, Computer code BCONT 2.1: A Computer Program for Calculating Bound→Continuum Transition Intensities for Diatomic Molecules, Chemical Physics Research Report No. CP-650R, University of Waterloo, 2002.
[58] M. Raab, G. Höning, W. Demtröder, and C. R. Vidal, J. Chem. Phys. **76**, 4370 (1982).
[59] U. Diemer, J. Gress, and W. Demtröder, Chem. Phys. Lett. **178**, 330 (1991).
[60] J. Huennekens, R. K. Namiotka, J. Sagle, Z. J. Jabbour, and M. Allegrini, Phys. Rev. A **51**, 4472 (1995).
[61] O. Kaufmann, A. Ekers, K. Bergmann, N. Bezuglov, K. Miculis, M. Auzinsh, and W. Meyer, J. Chem. Phys. **119**, 3174 (2003).
[62] C. G. Carrington, D. N. Stacey, and J. Cooper, J. Phys. B **6**, 417 (1973).